



Multi-wavelength diagnostics of precursor phase in solar flares

Arun K. Awasthi* and Rajmal Jain

Astronomy & Astrophysics Division, Physical Research Laboratory, Navrangpura, Ahmedabad, Gujarat 380 009, India

Abstract. In order to study the origin of precursor phase emission in solar flares and its relation to main phase energy release, we employ X-ray and EUV wavebands observations in 13 flare events observed during the years 2003-2004. The X-ray spectral mode observations are taken from “Solar X-ray Spectrometer (SOXS)” as well as RHESSI missions and EUV observations from TRACE mission. The X-ray emission spectral mode analysis revealed that, during precursor phase emission, the plasma temperature (T) and emission measure (EM) vary between 7–15 MK and $0.002 - 0.08 \times 10^{49} \text{ cm}^{-3}$ respectively. We report two major conclusions: (1) The precursor phase emission is originated from low-temperature and moderately dense plasma. (2) the precursor phase emission corresponds to low-altitude coronal loops, however, in co-spatial with the main phase energy release site. Further, during the study, we have also found some preliminary conclusions *viz.* (1) Isothermal plasma behavior in precursor phase and (2) Absence of high energy emission during precursor phase emission.

Keywords : Sun: flares – Sun: corona – Sun: X-rays

1. Introduction

Solar flares are sudden bursts in the atmosphere of the Sun releasing typically, 10^{32} ergs of energy. Theoretical and in some extent observational established process explaining this enormous amount of energy release start with the acceleration of charged particles following the reconnection of overlying magnetic field lines. These accelerated particles (majorly electrons) interact with both ambient electrons and ions, but

*email: awasthi@prl.res.in

lose most of their energy through coulomb collisions when they hit the chromosphere and emit thick-target also known as hard X-rays (HXR). These electrons via coulomb collision heat the chromosphere, which enhances the local pressure and thereby drives the heated plasma material up into the coronal loops which appear in form of soft X-rays (SXR) as a result of thin-target bremsstrahlung. Such a model, despite its overall elegance and self-consistency, does lead to important considerations concerning the importance of various auxiliary processes of the energy transport. For instance, it happens quite often that the SXR emission in flares starts a few minutes earlier than the HXR emission (termed as precursor phase), the maximum of the SXR emission occurs much later after the end of the HXR event (Veronig et al. 2002). The anomaly between theoretical models and observational evidences related to this precursor phase further enhanced in context to recent investigations by Battaglia, Fletcher & Benz (2009); Rudawy, Siarkowski & Falewicz (2010); Falewicz, Siarkowski & Rudawy (2011). Falewicz et al. (2011), in their study concluded that energy delivered by Non-Thermal electrons (NTEs) was fully sufficient to fulfill the energy budgets of the plasma during the pre-heating and impulsive phases of both flares as well as during the decay phase of one of them. They therefore concluded that there was no need to use any additional ad hoc heating mechanisms other than heating by NTEs. On the other hand, Battaglia et al. (2009), concluded by the study of the precursor phase of four solar flares observed by RHESSI mission to be consistent with chromospheric evaporation driven by a saturated heat flux. They added continuous heating in the corona to be necessary for sustaining the observed temperature.

In this regard, we study qualitative and quantitative parameters of solar flare plasma in the precursor phase of emission to explore the origin of this emission and their role in triggering the main phase emission.

2. Data analysis and results

2.1 X-ray emission in precursor phase

We employ the high resolution observation of 13 Solar flare events observed by SOXS mission which was launched onboard the GSAT-2 Indian spacecraft in 2003 (Jain et al. 2005). The Si detector of SOXS mission provides unprecedented resolution (0.7 keV) in the 4-25 keV energy range. We estimate the flare plasma's parameters during the precursor phase emission *viz.* temperature (T) and emission measure (EM) by employing the X-ray emission in solar flare in 4-12 keV energy band. The precursor phase is termed as a SXR excrescence, predominantly in ≤ 12 keV energy band before the flare main phase emission commencement. The data employed for the current investigation is obtained from URL <http://www.pr1.res.in/~soxs-data/DataHome.php>. The observed spectra are analyzed by forward fitting the isothermal function provided under Object Spectral Executive (OSPEX) package in SOLAR-SOFT (SSW) distribution. The OSPEX is an object-oriented interface for X-ray spectral analysis of solar data. Through OSPEX, the user reads and displays the input data,

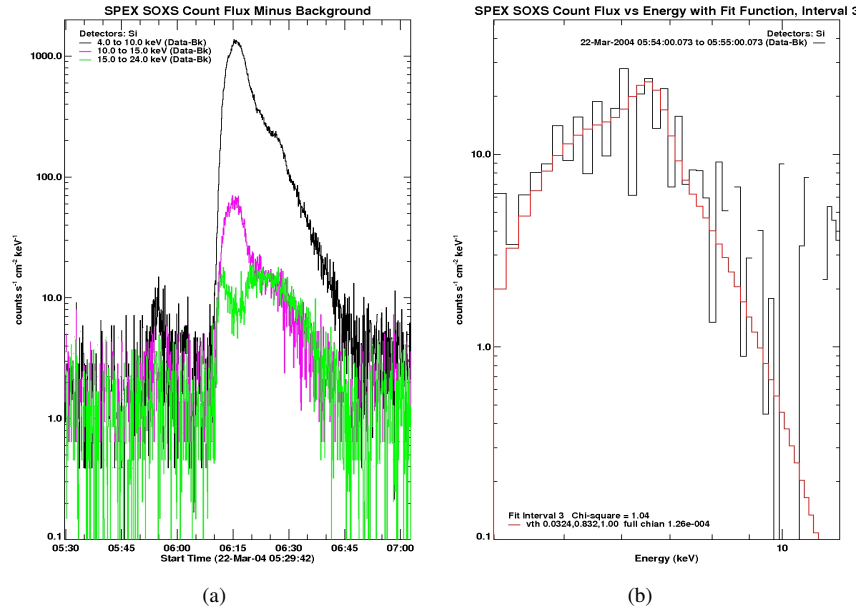


Figure 1. Left panel: The temporal evolution of the flare event which occurred on March 22, 2004. Right panel: The spectral evolution of the March 22, 2004 flare event in the energy range of 4-12 keV as observed by the Si detector onboard the SOXS mission (shown by black line). The model photon flux generated by employing isothermal function is shown by red line.

selects and subtracts background, selects time intervals of interest, selects a combination of photon flux model components to describe the data, and fits those components to the spectrum in each time interval selected. For the current study, we analyzed the spectra of 1-min time integration. During the fitting process, the response matrix is used to convert the photon model to the model counts to compare with the input count data. The resulting time-ordered fit parameters are stored and can be displayed and analyzed with OSPEX. The entire OSPEX session can be saved in the form of a script and the fit results stored in the form of a FITS file. The OSPEX enables us to look at the temporal evolution, spectrogram and spectral evolution. It also enables us to fit energy spectra using CHIANTI codes (Dere et al. 1997) for flare plasma diagnostics with the application of various thermal, line emission, multi-thermal, and non-thermal functions. Thus to calculate flare plasma temperature, emission measure (EM) and power law index (δ) etc., we have employed the least χ^2 fitting to the SOXS X-ray emission spectra in the OSPEX as described earlier by Jain, Aggarwal & Sharma (2008). In general, as the flare plasma is reported to be multi-thermal in nature (Jain et al. 2011), the observed flare photon spectra, therefore, should be best fitted by multi-thermal photon model. However, the photon flux during the precursor phase was best fitted with the help of isothermal function and therefore suggests an isothermal plasma content at precursor phase site. Left panel of Fig. 1 shows the temporal evolution of

the flare event occurred on March 22, 2004. A small bump in the evolution curve peaking at 05:54:00 UT is the precursor phase emission. The precursor phase leveled off at 06:05:00 UT. Later at 06:08:00 UT, the main phase emission in the event has taken place which peaks around 06:15:00 UT. Right panel of Fig. 1 shows the spectral evolution of the March 22, 2004 flare event in the energy range of 4-12 keV (shown by black line) during 05:54:00 - 05:55:00 UT. The observed spectra (red line) is fitted with the isothermal model (red line) with the goodness of fit represented by $\chi^2=1.04$. The estimated temperature and emission measures are 9.65 MK and $0.0324 \times 10^{49} \text{ cm}^{-3}$ respectively. The fitting parameters thus enable us to obtain the flare plasma parameters *viz.* temperature and emission measure as listed in Table 1.

The plasma parameters (*c.f.* Table 1) reveal low-temperature and moderate emission measure in the precursor phase. Further, in order to establish spatial relation between the precursor phase to the main phase emission, we employ the observations from RHESSI mission (Lin et al. 2002). RHESSI has nine coaxial germanium detectors, which record an X-ray emission from the full solar disk in a wide energy range (3 keV-17 MeV) with high temporal and energy resolutions as well as with a high signal sensitivity. Such characteristics allow a restoration of the 2D images and spectra in the X-ray band and provide very valuable data for investigation of the non-thermal emission of the solar flares. The images during the precursor and main phase emission of flare events under consideration are obtained using RHESSI data collected with sub-collimators 2F, 3F, 4F, 5F, 6F, 8F and 9F, with spatial resolution of 1 pixel, integrated over 30s duration, in the energy band of 6-7, 7-8, 8-9, 9-10, 10-12, 12-14, ... 48-50 keV energy band employing the CLEAN imaging algorithm. The reconstructed images thus enabled us to visualize the location of the precursor and main phase emission. Fig. 2 shows the series of images at the time of peak of precursor phase *i.e.* at 05:54:00 - 05:54:30 UT in different energy bands *viz.* 6-7, 7-8, 8-9, 9-10, 10-12 and 12-14 keV. Fig. 3 shows the series of images at main phase emission *i.e.* at 06:44:00 - 06:44:30 UT in the energy band same as above. The images at the precursor and main phase reveal the co-spatiality of the emission. In addition, we note the emission in precursor phase is visible only in low-energy band *i.e.* between 6-12 keV in contrast to the main phase emission which reaches the value of 20-22 keV energy band. The same analysis performed on the events under current investigation reveals the co-spatial origin of precursor phase emission in all flares except one. Table 1 shows the statistics of the results revealed by the reconstructed images.

2.2 EUV emission in precursor phase

In view of the low-temperature plasma giving rise to precursor phase emission, we further explore the plasma characteristics by employing EUV observations from TRACE

Table 1. The precursor phase emission characteristics.

Date	Start Time (UT)	Peak Time (UT)	End Time (UT)	Temperature (MK)	EM ($\times 10^{49} \text{ cm}^{-3}$)	Spatial Relation with main phase
10 Jul 2003	04:23	04:27	04:32	11.02	0.027	Co-spatial
11 Jul 2003	04:19	04:22	Flare started	12.41	0.022	Not co-spatial
17 Nov 2003	04:55	05:06	05:18	11.05	0.012	Co-spatial
18 Nov 2003	05:08	05:15	05:24	9.98	0.061	Co-spatial
23 Nov 2003	03:51	03:55	Flare started	11.55	0.019	Co-spatial
21 Dec 2003	04:10	04:12	Flare started	11.83	0.017	Co-spatial
10 Jan 2004	04:13	04:15	04:18	9.98	0.024	Co-spatial
01 Feb 2004	05:58	06:00	06:03	10.91	0.017	Co-spatial
26 Feb 2004	05:31	05:31	Flare started	9.39	0.049	Co-spatial
22 Mar 2004	05:49	05:54	06:06	9.65	0.032	Co-spatial
13 Jul 2004 - I	04:24	04:30	Flare started	13.92	0.005	Co-spatial
13 Jul 2004 - II	05:21	05:26	Flare started	16.58	0.007	Co-spatial
14 Jul 2004 - I	05:02	05:06	05:11	11.36	0.027	Co-spatial
14 Jul 2004 - II	05:15	05:17	05:17	11.83	0.032	Co-spatial
14 Aug 2004	04:00	04:05	04:11	9.744	0.046	Not co-spatial/ Same AR

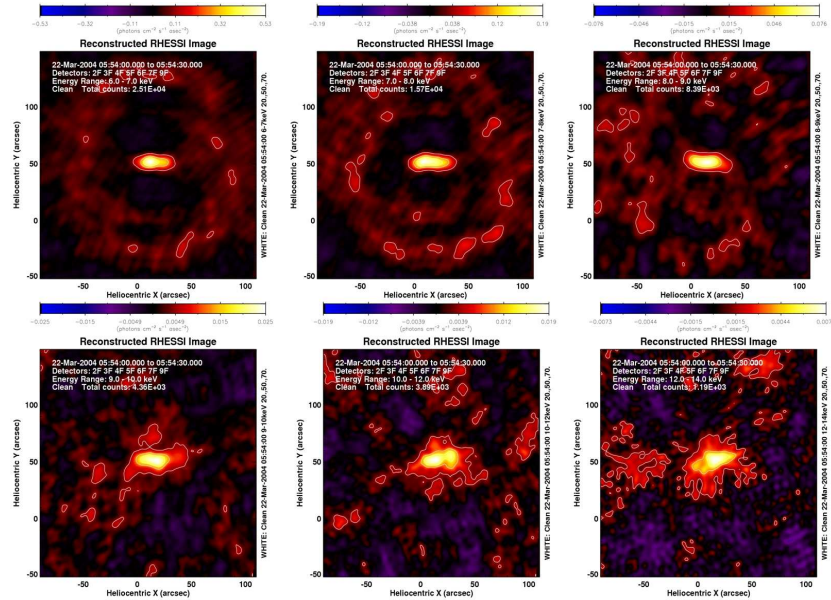


Figure 2. Series of images at the peak time of precursor phase *i.e.* at 05:54:00 - 05:54:30 UT in different energy bands *viz.* 6-7, 7-8, 8-9, 9-10, 10-12 and 12-14 keV

mission in 171 Å and 195 Å. We apply the standard routines provided in SSW and described at http://www.mssl.ucl.ac.uk/surf/guides/tag/tag_top.html to process TRACE observations. The processed images are then subtracted from a background image to observe the changes at the time of preflare and main flare emission where background image is considered as the image taken prior to the precursor phase emission commencement. Fig. 4 shows the times series of images for the event occurred on March 22, 2004, observed in 171 Å. In this case, the image at 05:45:00 UT is considered as the background image. We then subtracted the observed time series of images at the precursor and main phase of emission with the background. Left panel of Fig.3 shows the difference image at the peak of precursor phase emission *i.e.* at 05:54 UT on March 22, 2004, middle panel shows the difference image at the leveled off time of precursor phase emission *i.e.* at 06:06 UT and right panel shows the difference image at peak of the main phase emission *i.e.* at 06:15:00 UT (*c.f.* Left panel - Fig.1). It may be noted from Fig.3 that the emission in precursor phase is co-spatial to the main phase, however, originated from low altitude loops.

3. Discussion and conclusion

The current investigation, focused on the origin of precursor phase emission and its relationship with the main phase emission, reveals the co-spatial nature. In addition,

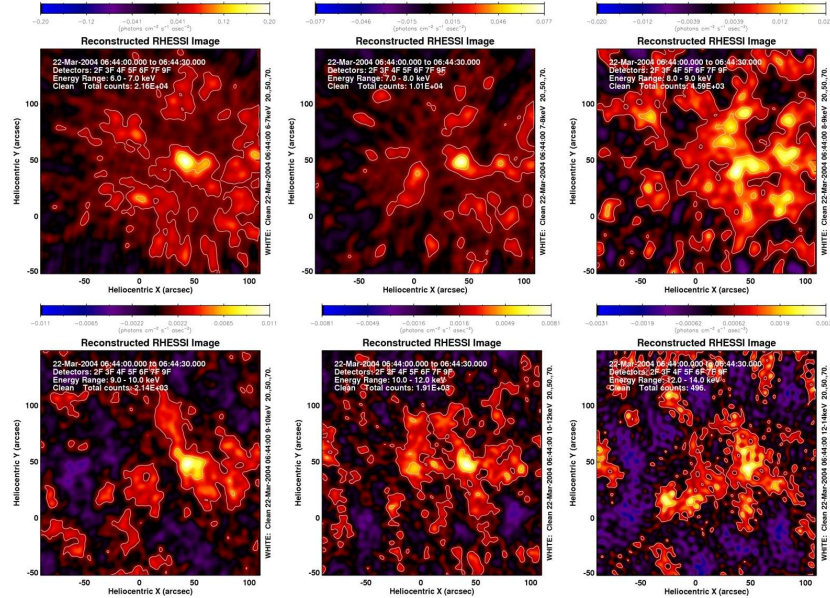


Figure 3. Series of images at the peak time of main phase i.e. at 05:54:00 - 05:54:30 UT in different energy bands *viz.* 6-7, 7-8, 8-9, 9-10, 10-12 and 12-14 keV

we report the low-temperature and moderately dense plasma at the time of precursor phase. We discuss some open issues encountered during the study.

3.1 Isothermal versus multi-thermal plasma in the precursor phase

We employed the 1-1 min integrated spectra at the time of precursor phase emission employing the isothermal function to estimate the flare plasma temperature. However, for comparison, we have also made the forward fitting of the photon spectra of the same time employing the multi-thermal function provided in OSPEX/SSW. The flare plasma temperature after best fitting with multi-thermal model is estimated to be 30-50 MK. This high temperature in the chromosphere (density 10^{12}cm^{-3}) is only possible when the chromospheric evaporation is driven by non-thermal electrons (NTEs) energized by the magnetic reconnection and therefore the SXR emission even at the precursor phase must accompany HXR. In this regard, the unavailability of HXR emission indirectly suggests the unphysical solution in form of temperature estimation by multi-thermal function. On the other hand, the temperature values estimated after the fitting performed on the observations employing isothermal function ranges between 7–15 MK which is remarkably less than that estimated by employing multi-thermal function. The plasma of 7–15 MK can be produced by the process of plasma heat-

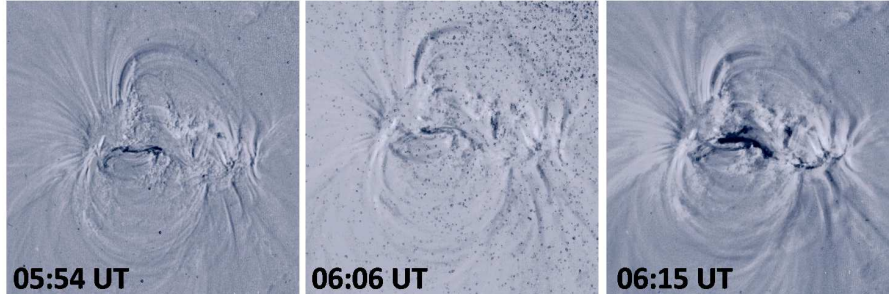


Figure 4. Time series of difference images in 171 \AA from TRACE observation for the flare event of 22 March 2004 . Left panel: Difference image @ 05:54UT, the peak time of precursor phase emission. Middle panel: Difference image @ 06:06 UT, the quiet time between precursor phase and main phase energy release. Right panel: Difference image @ 06:15 UT, corresponding to main flare peak time.

ing without NTEs (No HXR). Therefore we can consider the flare plasma in the precursor phase of emission to be isothermal in nature.

3.2 Beam-driven versus conduction-driven chromospheric evaporation

Rephrasing the debate on the precursor phase emission, two kind of physical processes are made responsible *viz.* the beam-driven heating of chromosphere (Falewicz et al. 2011) and conduction-driven chromosphere heating (Battaglia et al. 2009). In our investigation, at the precursor phase, the plasma appears to be emitting only in the low energy. Therefore the preliminary inferences we may draw are as follows:

- This emission is originated by the chromospheric plasma heated by conduction driven coronal electrons which do not have sufficient energy to produce HXR.
- This emission is originated by the chromospheric plasma heated by beam-driven coronal electrons but the limited sensitivity of the instruments in the regime of high energy due to inevitably low signal-to-noise ratio might have suppressed the HXR in the precursor phase.
- This emission is originated in low-altitude reconnection given by destabilizing filament or prominence as also found by in few events by Chifor et al. (2007) showing precursor phase. The $H\alpha$ observation therefore may shed light on this possibility and is the future scope of current study.

Acknowledgements

Authors would like to acknowledge Dept. of Space (Govt. of India).

References

- Battaglia M., Fletcher L., Benz A. O., 2009, *A&A*, 498, 891
Brown J. C., 1971, *Solar Phys.*, 18, 489
Chifor C., Tripathi D., Mason H. E., Dennis B. R., 2007, *A&A*, 472, 967
Dere K. P., Landi E., Mason H. E., Monsignori Fossi B. C., Young P. R., 1997, *A&AS*, 125, 149
Falewicz R., Siarkowski M., Rudawy P., 2011, *ApJ*, 733, 37
Jain R., Aggarwal M., Sharma R., 2008, *JApA*, 29, 125
Jain R., et al., 2005, *Solar Phys.*, 227, 89
Jain R., Awasthi A. K., Rajpurohit A. S., Aschwanden M. J., 2011, *Solar Phys.*, 270, 137
Lin R. P., et al., 2002, *Solar Phys.*, 210, 3
Rudawy P., Siarkowski M., Falewicz R., 2010, *IAUS*, 264, 282
Veronig A., Vršnak B., Temmer M., Hanslmeier A., 2002, *Solar Phys.*, 208, 297